

Observations of Galaxies at $z \gtrsim 10$ Allow to Test Cosmological Models with Features in the Initial Power Spectrum

S. V. Pilipenko,^{1,*} S. A. Drozdov,¹ M. V. Tkachev,¹ A. G. Doroshkevich^{1,2}

¹*P.N. Lebedev Physical Institute, Astro Space Center, Moscow, 117997 Russia*

²*National research centre Kurchatov institute, Moscow, Russia*

The initial power spectrum of density perturbations, generated during the inflationary epoch, is now constrained by observations on scales $\lambda > 5$ Mpc and has a power-law form. The peculiarities of the inflationary process can lead to the appearance of non-power-law contributions to this spectrum, such as peaks. The exact size and shape of the peak cannot be predicted in advance. In this paper, we propose methods for searching for such peaks in the region of the spectrum with $\lambda < 5$ Mpc. Perturbations on these scales enter the nonlinear stage at $z \gtrsim 10$, which is now becoming accessible to observations. Our studies of numerical models of large-scale structure with peaks in the initial spectrum have shown that spectral features on scales with $\lambda > 0.1$ Mpc manifest in the clustering of galaxies, as well as affect their mass function, sizes, and density. Studying these characteristics of distant galaxies will allow us to constrain cosmological models with peaks.

Ключевые слова: (cosmology:) large-scale structure of the Universe—galaxies: high redshifts

1. INTRODUCTION

In the currently accepted cosmological model, the initial power spectrum of density perturbations has a shape devoid of preferred scales, close to that predicted by Harrison and Zeldovich (Harrison 1970, Zeldovich 1972), $P \propto k^{0.961}$ (Planck Collaboration et al. 2020). According to observations of the relic radiation and the distribution of galaxies in space, this spectrum is verified up to a scale of $k \approx 1$ h/Mpc¹ (Chabanier et al. 2019). Although such a spectrum emerges even in the simplest inflation models, there are more complex models where the spectrum may not have a power-law shape. In particular, models with one or several peaks in the primordial spectrum were invented due to the growing interest in the topic of primordial black holes. A review of inflationary models with peaks is given in the article Inomata et al. (2023). Also the power spectrum can acquire a peak in the models with a primordial magnetic field, see, e.g. Ralegankar et al. (2024) or in Brans-Dicke gravity (Sletmoen and Winther 2024). Models with peaks in the spectrum have not gained much popularity due to the requirement of introducing new parameters in cosmology. However, the development of

observation techniques for galaxies with redshifts $z > 10$ opens up the possibility of constraining the peaks at $1 < k < 100$ h/Mpc in the near future, which served as motivation for this work.

A peak in the spectrum, i.e., increased power of perturbations in a certain range of scales, will lead to the early formation of a network of walls and filaments of the structure on the corresponding scales, as well as to the early appearance of gravitationally bound objects – dark matter halos, some of which may contain galaxies. Therefore, it is obvious that manifestations of the peak should be sought in the distribution of halos by mass (mass function), and in the spatial distribution of galaxies.

The halo mass function is available for study both by simple analytical methods, such as Press-Schechter theory or its refinements (Despali et al. 2016, Press and Schechter 1974, Sheth and Tormen 1999), and by numerical models. For spectra with a peak, the mass function was first investigated using numerical models in the work Knebe et al. (2001), however, the position of the peak in it corresponded to the masses of galaxy clusters, which is already closed by observations. In the range of scales and redshifts of interest to us, the mass function was investigated in Padmanabhan and Loeb (2023) using the Press-Schechter formalism and in Tkachev et al. (2024) using numerical models.

* spilipenko@asc.rssi.ru

¹ Here and below $h = H/100$ km/s/Mpc

As shown in Tkachev et al. (2024), information about the peak in the spectrum appears in the mass function only at sufficiently large redshifts, $z \geq 10$. In later epochs, numerous halos generated by the peak in the spectrum become part of more massive and later formed halos, so that by $z = 0$ the mass function of isolated halos in the model with a peak almost does not differ from the mass function for the model with a power-law spectrum. In other words, perturbations in the range of scales $1 < k < 100 \, h/\text{Mpc}$ enter the nonlinear stage at $z \geq 10$, and at lower redshifts one has to deal with a substantially nonlinear structure in which the memory of the initial conditions is largely erased by the previous evolution of these perturbations. It is also superimposed on the complex evolution of baryonic matter, which complicates the interpretation of observations, for example, see the discussion of the properties of the Ly- α forest (Demiański et al. 2022), discussions of the problem of the lack of satellites (Brooks et al. 2013, Klypin et al. 1999, Sawala et al. 2016). Therefore, it is observations of objects at high redshifts that should be used to measure the power spectrum at small scales.

Recent observations on the James Webb Space Telescope (JWST) have led to the discovery of a population of galaxies at redshifts $z > 10$ (Castellano et al. 2022, Donnan et al. 2023, Finkelstein et al. 2022, Labbé et al. 2023, Naidu et al. 2022). A number of authors claim that there is an excess of massive galaxies compared to the standard model (Boylan-Kolchin 2023, Lovell et al. 2022), others say that there is no excess (Chen et al. 2023, Prada et al. 2023, Shen et al. 2023). At the same time one should note that for distant galaxies, not the dynamic mass is determined, but only the spectral energy distribution, which is then translated into stellar mass using models of stellar evolution. By setting the parameter of star formation efficiency ϵ (the fraction of baryonic matter that has turned into stars), one can estimate the mass of baryons, and from it, through the cosmological ratio of baryonic and dark matter, the total mass. Such an assessment contains several sources of uncertainty: the efficiency of star formation can vary widely, the share of baryons in a separate halo

may differ from the average for the Universe. For this reason (since we do not have a reliable theory of galaxy formation that allows us to unambiguously find their parameters from visible spectra), it is still impossible to draw unambiguous conclusions about the discrepancy between observations and ΛCDM cosmology. Attempts to test cosmology using these observations are still limited to restrictions on ϵ , for example, Xiao et al. (2023) found three massive galaxies at $z \sim 5-6$, which in the ΛCDM model require an unrealistic value of $\epsilon > 0.2$.

In the works Padmanabhan and Loeb (2023), Tkachev et al. (2024) it was shown that adding a peak to the power spectrum can reduce this possible contradiction between observations and cosmology, reducing the value of ϵ required to explain the observations. Thus, according to Tkachev et al. (2024), in the model with a peak for all the galaxies considered in this article, $\epsilon < 0.1$ is sufficient, which is consistent with known data on the efficiency of star formation (Behroozi and Silk 2018, Giodini et al. 2009, Lovell et al. 2022).

Changing the power spectrum of perturbations not only changes the mass function, but also gives a number of other predictions that, in our opinion, will allow these models to be tested: changes in the large-scale structure and changes in the structure of halos (and galaxies) due to their earlier formation. These two predictions are analyzed in this work. To study the nonlinear evolution of the structure, we performed numerical simulations of the N-body problem for a medium of dark matter (cosmological simulations). Due to the fact that the processes of galaxy formation at $z > 10$ are not modeled reliably enough now, we consider only dark halos. Not all of them can contain galaxies, also the luminosity of a galaxy does not have to be proportional to the mass of the halo, which leads to some observational selection of halos. For simplicity, in our work, we consider all halos with a mass above a certain threshold, we leave the modeling of galaxy formation and selection processes for future research.

The spatial distribution of galaxies or halos can be described quantitatively using the minimal spanning tree (MST) method (Barrow et al.

1985, Doroshkevich et al. 2004). This method connects objects (halos or galaxies) in space with segments so that one can “travel” from one object to any other in a unique path, and the total length of the segments is minimal. The distribution of the lengths of the MST segments is one of the characteristics of the spatial distribution, in particular, it allows to distinguish systems of objects distributed randomly in three-dimensional space from those strung on randomly located planes or straight lines in space (which resembles a network of pancakes or filaments of large-scale structure). By setting a certain threshold length of the segment and discarding all longer segments, we can obtain a system of clusters – sub-volumes of increased density of objects. These clusters can also be divided into filaments and pancakes according to some signs (Demiański and Doroshkevich 2004, Doroshkevich et al. 2001). In our work, we also apply the MST method to study halo clustering at $z \sim 10$.

To describe the internal structure of halos, we adhere to the concept outlined in the article Demiański et al. (2023). The halo is approximately considered as a spherically symmetric system in which matter is distributed according to the Navarro-Frenk-White (NFW) density profile. This profile is characterized by two parameters, which are convenient to use as the maximum circular velocity v_{max} and the value defined in Demiański et al. (2023) $w \equiv v_{max}/r_{max}$, where r_{max} is the radius at which the maximum circular velocity is reached. For comparison, we also use another description popular in the literature in terms of virial mass M_v and concentration parameter $c \equiv r_v/r_s$, where r_v is the virial radius of the halo (the radius within which the average density is $\Delta \approx 200$ times higher than the critical density of the Universe, which corresponds to the satisfaction of the virial relation for the spherical model Bryan and Norman (1998)), and $r_s \approx r_{max}/2.2$ is the characteristic radius of the NFW density profile inflection.

2. NUMERICAL MODELS

Various scenarios of cosmological inflation lead to the formation of spectra of complex

shape, sometimes including numerous peaks on different scales, (see, for example, Ivanov et al. 1994). In order not to be tied to a specific model of inflation, we describe the peak with the simplest form – a Gaussian curve (in logarithmic coordinates), which is characterized by the position of the center of the peak k_0 , its amplitude A and width σ_k :

$$P_{\text{bump}}(k) = P_{\Lambda\text{CDM}}(k) \times \left(1 + A \exp\left(-\frac{(\log(k) - \log(k_0))^2}{\sigma_k^2}\right)\right). \quad (1)$$

At the same time, for the case of narrow peaks with $\sigma_k < 1$, physical responses, for example, the mass function, will depend only on the product of amplitude and width, i.e., on the integral under the curve (1). Therefore, we further fix the width of the Gaussian $\sigma_k = 0.1$ and change only its position and amplitude.

In the work by Tkachev et al. (2024), an analysis of different amplitudes and positions of Gaussians was conducted, demonstrating that the variant with $k_0 = 7 \text{ h/Mpc}$, $A = 20$, $\sigma_k = 0.1$ allows explaining a possible excess of galaxies at high redshifts under reasonable assumptions about the efficiency of star formation, $\epsilon < 0.1$. In this study, we analyze this variant and all other peak variants for which numerical models were computed in Tkachev et al. (2024). The parameters of the models are presented in Table 1. Numerical models cover the range of the parameter k_0 from 7 to 80 h/Mpc and are named according to the value of the parameter k_0 .

The parameters of the numerical models used are described in detail in the work Tkachev et al. (2024), a brief description is given here. Initial conditions for the models are set at $z = 300 - 1000$ in the form of a random realization of a Gaussian field of peculiar velocities. Particle positions are obtained from velocities in accordance with the approximate Zeldovich theory. At the same time, the same realization of a sequence of random numbers is used for all models, which eliminates random differences between models. The calculation of further evolution was performed by the GADGET-2 code (Springel 2005) up to a redshift of $z = 8$. Since the size of the model cube is small, 5 Mpc/h , the

Table 1. Parameters of numerical models

Model	Λ CDM	k7	k15	k30	k80
Cube size (Mpc/ h)	5.0	5.0	5.0	5.0	5.0
N_{total} (particles)	512^3	512^3	512^3	512^3	512^3
Initial redshift	300	10^3	10^3	10^3	10^3
Final redshift	8	8	8	8	8
Peak position k_0 (h/Mpc)	–	7	15	30	80
Peak amplitude A	0	20	20	20	10
Peak width σ_k	–	0.1	0.1	0.1	0.1

calculation cannot be extended to lower redshifts (boundary conditions start to influence the non-linear evolution of mass distribution). On the other hand, the small size of the cube allowed resolving scales corresponding to all considered peaks in the spectrum since the Nyquist wave number $k_N \approx 320 \text{ } h/\text{Mpc} \gg k_0$ for all models. Dark matter halos were identified by the Amiga Halo Finder code (Knollmann and Knebe 2009) using the standard density criterion.

An overall understanding of the evolution of matter distribution in the calculations can be obtained from Fig. 1. It shows the initial power spectrum of density perturbations and its evolution over time for the k15 model. The ordinate axis represents the dimensionless quantity $k^3 P(k)$ characterizing the amplitude of density perturbations on a scale of $2\pi/k$. Perturbations become nonlinear when this amplitude reaches unity. In this numerical model, this first occurs around $z \approx 100$ for perturbations at the scale of the peak, $k = 15 \text{ } h/\text{Mpc}$. Halos with masses of $10^6 - 10^7 \text{ } M_\odot/h$ form at $z = 36$. Halos with a mass of $10^9 \text{ } M_\odot/h$ appear at $z = 18$, roughly corresponding to the scale of the peak in the spectrum, and perturbations with $k > 10 \text{ } h/\text{Mpc}$ become predominantly nonlinear. By $z = 8$, perturbations on the scale of the cube become nonlinear, indicating no need to continue further calculations.

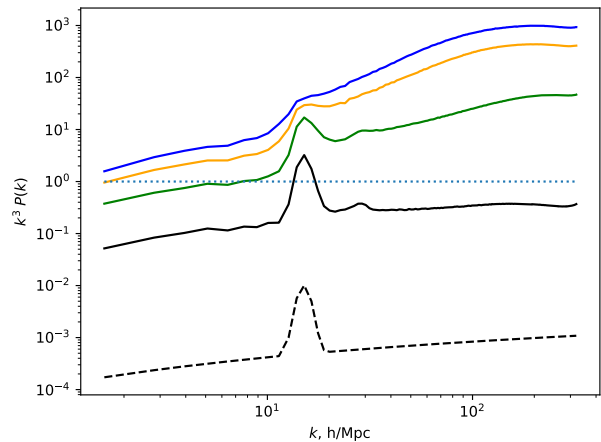


Figure 1. The power spectrum of density perturbations in the numerical model k15. Dashed line – initial spectrum at $z = 1000$. Solid lines – at $z = 50, 18, 11, 8$ (bottom to top). Dotted line – the boundary of linear and nonlinear perturbations.

3. LARGE-SCALE STRUCTURE

According to the theory proposed by Zel'dovich (Zel'dovich 1970), cosmological perturbations lead to the formation of a network of walls (pancakes), filaments and voids between them. An increase in power in a certain range of scales leads to an increase in density contrast and an earlier formation of this structure on the corresponding scales. In the k7 model, the peak on the spectrum is located on a linear scale of $0.9 \text{ Mpc}/h$, which at $z = 10$ corresponds to an angular scale of 5.2 arc minutes, and in this model,

one can expect the manifestation of observable structures from galaxies of such sizes. For comparison, the field of view of the most sensitive NIRCcam camera on JWST is $2.25' \times 2.25'$, i.e., such scales are available in existing and planned surveys of distant galaxies. It is also interesting to note the recent work Wang et al. (2023), in which a filament about 10 Mpc in size was discovered at $z = 6.6$, which suggests that the study of large-scale structure in the distribution of galaxies at large z is a solvable problem.

The type of large-scale distribution of galaxies for models with a peak in the spectrum is demonstrated in Fig.2. 1000 most massive halos from each model have been selected. The surface density of objects in Fig.2 roughly corresponds to the observed surface density of distant galaxies with $z \geq 10$ in existing JWST surveys: here 1.1 galaxies per square minute, 0.4 galaxies per square minute in the sample from the work Donnan et al. (2023), 1.1 galaxies per square minute in the survey from the article Bradley et al. (2023). However, in real surveys, a large range of redshifts is covered, while in Fig.2 the depth of the image is only 5 Mpc/h. Nevertheless, this illustration clearly shows the difference between the Λ CDM and k7 models. As k_0 increases, the differences gradually disappear: the cellular structure caused by the introduction of the peak shifts to the region of scales of individual galaxies.

To quantitatively describe the large-scale structure, we used the MST method, which gives several characteristics of the spatial distribution of objects. The first such characteristic is the distribution function of the lengths of the segments that make up the tree, $P(\ell)$. The average and median values of the length and their distribution functions for the 1000 and 3000 most massive halos from the models under consideration are presented in Table 2 and in Fig. 3. From these results, it can be seen that the k30 model demonstrates a distribution function that is significantly different from both Λ CDM and other models.

Another characteristic that can be obtained using the tree is the branching of the tree, which allows to establish the proportion of filaments in the structure. To study this value, the tree

is first broken down into clusters by discarding all segments with a length greater than some ℓ_{thr} , as well as removing all clusters containing less than M_{thr} objects. Then each cluster is divided into a “trunk” – a set of segments that form the longest one-way path through the tree, and “tree” – segments that did not fall into the trunk. The ratio of the trunk length L_{trunk} to the total length of the segments of this cluster (trunk + branches) L_{tree} characterizes the degree of elongation of the cluster (Doroshkevich et al. 2001). Thus, filamentous structures should have $L_{trunk}/L_{tree} \approx 1$.

We used $\ell_{thr} = \ell_{med}$, $M_{thr} = 5$. This choice is due to the fact that with a minimum mass of 3 or less, it is impossible to split part of the tree into a trunk and branches, and the larger the mass of the cluster, the more original objects will have to be excluded from the analysis. The threshold length affects the number of clusters: if it is small, a significant part of the objects is thrown out of the analysis, if it is too large, the objects are combined into one or more large clusters (percolation occurs) and it is pointless to talk about the shape of such clusters. Small changes in threshold parameters (for example, $M_{thr} = 6$, $\ell_{thr} = 1.2\ell_{med}$) do not qualitatively affect the conclusions we have reached.

Consider a typical cluster with $M = 5$ points for our criterion. If they all form a trunk, obviously $L_{trunk}/L_{tree} = 1$, but if there is one branch, then $L_{trunk}/L_{tree} = 0.8$. Therefore, we will call filaments clusters with $L_{trunk}/L_{tree} \geq 0.8$. Distributions of the ratio L_{trunk}/L_{tree} are presented in Fig. 4, the legend indicates the proportion of filaments f (clusters with $L_{trunk}/L_{tree} \geq 0.8$). Based on these data, we can draw the following conclusions: in the k7 model for a sample of 1000 halos and in the k15 model for a sample of 3000 halos, there is an increased number of filaments with $L_{trunk}/L_{tree} > 0.8$ compared to the Λ CDM model, in the k30 model for a sample of 3000 halos – reduced, and in the k80 model comparable to Λ CDM. The dependence of the result on the sample of halos demonstrates the fact that by the distribution of halos one can see only the filaments of the large-scale structure, which are represented by a sufficiently large number of halos.

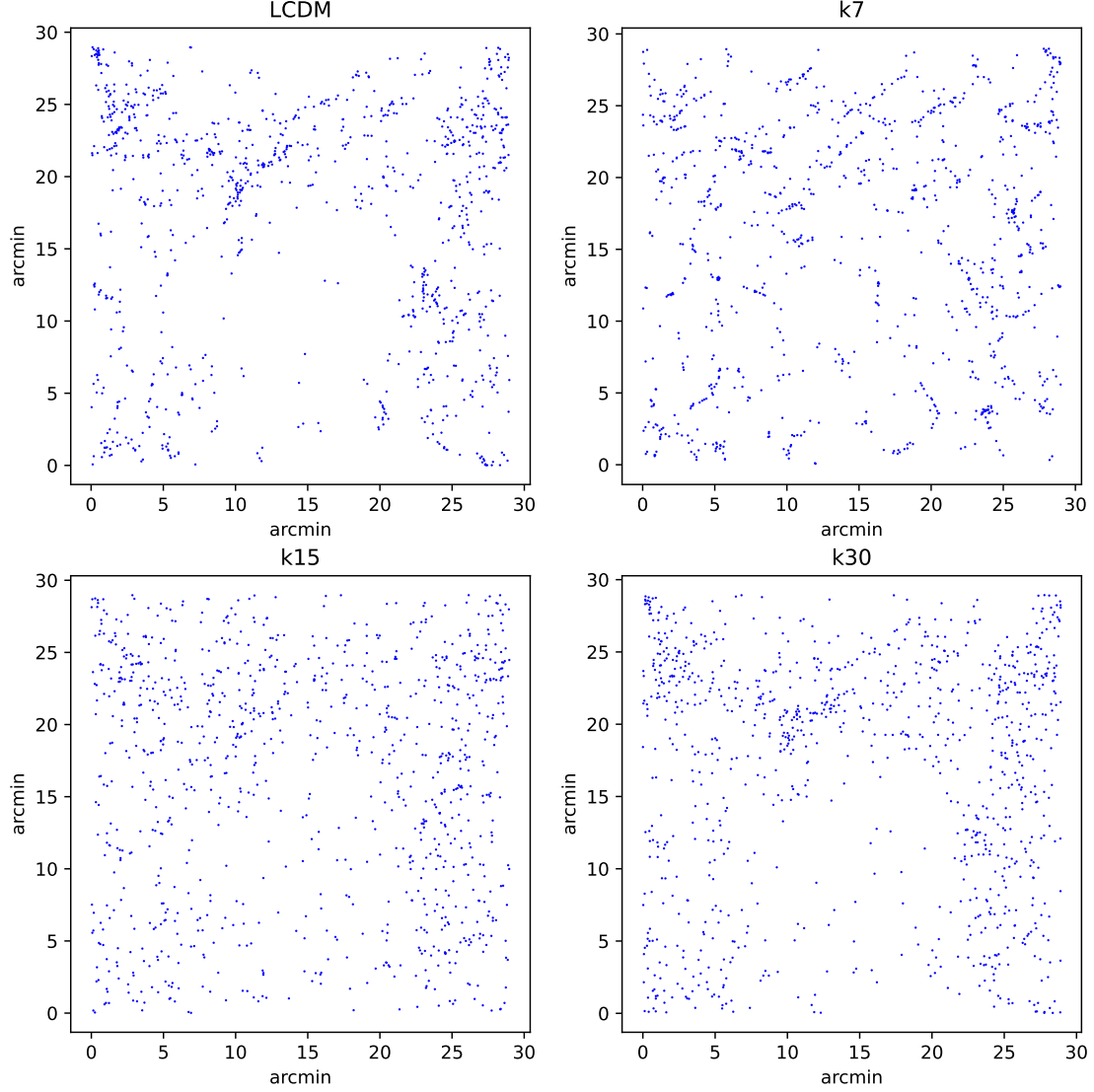


Figure 2. Spatial distribution of the 1000 most massive halos in numerical models at $z = 10$ in projection onto the celestial sphere.

Table 2. Average and median values of lengths of MST segments for samples of 1000 and 3000 most massive halos at $z = 10$.

Model	1000 halos		3000 halos	
	$\langle \ell \rangle$ (kpc/h)	ℓ_{med} (kpc/h)	$\langle \ell \rangle$ (kpc/h)	ℓ_{med} (kpc/h)
Λ CDM	175	117	114	79
k7	169	94	92	58
k15	288	302	160	109
k30	230	200	182	177
k80	163	99	109	71

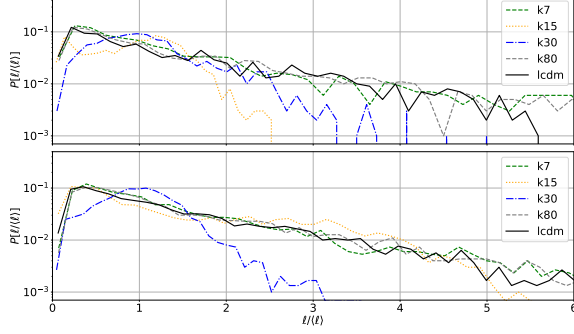


Figure 3. Distribution of lengths of MST segments for samples of 1000 most massive halos (top), and 3000 most massive halos (bottom panel) at $z = 10$ for five cosmological models.

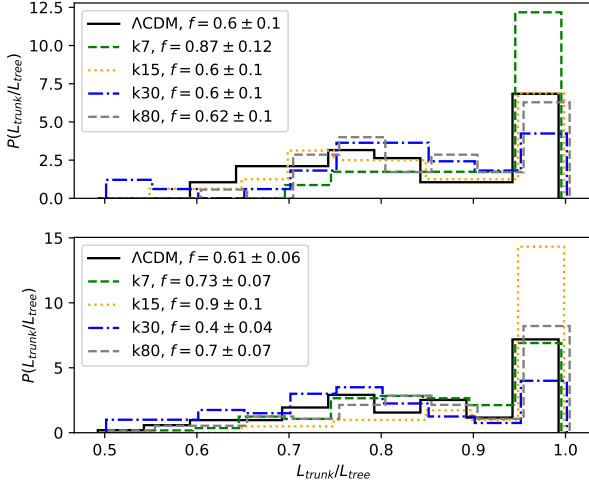


Figure 4. Distribution of the ratio of the length of the trunk of the tree to the total length of the tree L_{trunk}/L_{tree} for five cosmological models for samples of 1000 halos (upper graph) and 3000 halos (lower graph). The histograms are slightly offset along the horizontal axis to avoid overlapping lines.

4. STRUCTURE OF HALO

The work Demiański et al. (2023) presents a model for describing dark matter halos and compares halos from numerical models with observed galaxies. This model characterizes the halo by two parameters: the maximum circular velocity v_{max} and the density parameter w^2 :

² In the article Demiański et al. (2023), the value of w was denoted by the letter h . Characteristic density inside r_{max} : $1/4\pi Gw^2$.

$$v_{max} = \max \left(\sqrt{\frac{GM(r)}{r}} \right) \quad (2)$$

$$w = \frac{v_{max}}{r_{max}}. \quad (3)$$

This description is slightly different from that adopted in the literature on cosmological simulations, where two other characteristics are introduced: the virial mass M_v and the concentration parameter c (see, for example Klypin et al. 2011). The description in terms of c , M_v is convenient for simulations, but in observations, the virial radius is difficult to measure, since it is located on the periphery of the halo, where there is practically no visible matter. In addition, these parameters correlate with each other, so any selection effects that affect one parameter also affect the distribution of the second parameter. For example, we cannot talk about the distribution of the concentration parameter if we do not specify what range of virial mass we are talking about.

From the point of view of theory or simulations, these two descriptions are equivalent, since by setting the NFW density profile, we can switch from the parameters c , M_v to the parameters w , v_{max} or vice versa. In the work Demiański et al. (2023), the description of w , v_{max} was applied to observed galaxies, and it was shown that the parameters measured in observations for typical galaxies at $z \sim 0$ correspond to the parameters of halos from simulations, which demonstrates the applicability of such a description for comparing observations and theory.

The value of v_{max} characterizes the depth of the potential well created by the dark halo, which, in turn, is important for the first galaxies: the gas accreting onto the halo is heated to a temperature of the order of

$$T \approx \frac{\mu m_p v_{max}^2}{2k_b}, \quad (4)$$

where m_p is the mass of the proton, k_b is the Boltzmann constant, μ is the average molecular weight of the gas, $\mu = 1.22$ for neutral primary gas. If the halo has $v_{max} > 12$ km/s, then the gas in it will heat up to 10^4 K and ionize, which will allow the gas to effectively relieve energy and, as

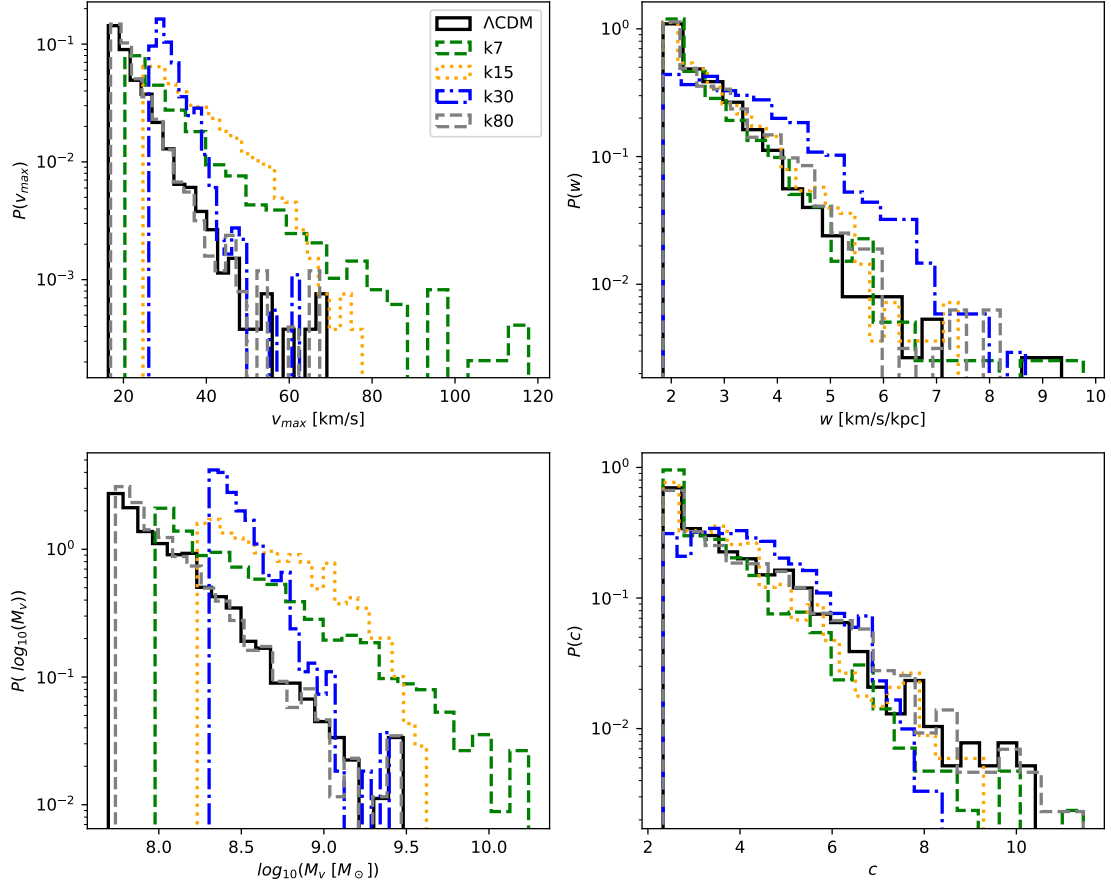


Figure 5. Histograms of the distribution of parameters of the 1000 most massive halos in 5 numerical models. Solid black line – model Λ CDM, black dashed – k7, black dotted – k15, black dash-dotted – k30, gray dashed – k80. *Top left panel:* maximum circular velocity v_{max} . *Top right panel:* halo density parameter $w = v_{max}/r_{max}$. *Bottom left panel:* logarithm of virial mass M_v . *Bottom right panel:* concentration parameter $c = r_v/r_s$.

a result, form stars (see, for example, Barkana and Loeb 2001, Haiman et al. 2000). The larger v_{max} , the more difficult it is to throw gas out of the galaxy as a result of supernova explosion processes, therefore, in halos with a large v_{max} there is more gas left for further star formation, and such halos can potentially contain galaxies with a larger stellar mass.

The value of w characterizes the density of matter inside the halo, the higher this value, the greater the density. The mean density inside r_{max} is $1/4\pi Gw^2$. Obviously, with the same v_{max} for two halos, w will be larger for the one for which the maximum circular velocity is reached at a smaller radius, i.e., halos with large w are more compact.

We selected 1000 of the most massive halos

from each of our numerical models. Histograms of the distribution of parameters v_{max} , w , M_v , c are presented in Fig.3. From these distributions, several conclusions can be drawn:

1. In all models, the considered halos have $v_{max} > 12$ km/s, which means that galaxies can arise in them.
2. Models k7, k15, and k30 demonstrate an excess of v_{max} velocities (as well as halo mass M_v) compared to Λ CDM. Galaxies in these models should also possess larger stellar masses than in Λ CDM. If it becomes possible to estimate the circular velocities of distant galaxies using spectroscopy, this can be used to test models with a peak at $k_0 \leq 15$ h /Mpc: in such

Table 3. Parameters of distributions v_{max} , w , M_v , and c at $z = 10.1$ in the numerical models studied.

Model	Λ CDM	k7	k15	k30	k80
Median v_{max} (km/s)	20.1	27.6	33.7	30.0	20.5
Average v_{max} (km/s)	22.2	31.9	36.3	31.2	22.4
Dispersion v_{max} (km/s)	6.3	13.4	9.6	4.2	6.1
Median w (hkm/s/kpc)	2.4	2.3	2.5	3.1	2.5
Average w (hkm/s/kpc)	2.6	2.6	2.7	3.3	2.7
Dispersion w (hkm/s/kpc)	0.9	1.0	0.9	1.1	0.9
Median M_v ($10^8 M_\odot/h$)	0.8	2.1	3.9	2.7	0.9
Average M_v ($10^8 M_\odot/h$)	1.4	5.7	6.0	3.2	1.4
Dispersion M_v ($10^8 M_\odot/h$)	2.2	13.4	5.5	1.8	2.1
Median c	3.4	3.0	3.4	4.0	3.4
Average c	3.8	3.4	3.6	4.1	3.9
Dispersion c	1.4	1.2	1.3	1.2	1.5

models, galaxies with $v_{max} > 100$ km/s may already be encountered at $z = 10$, while in Λ CDM, the detection of such galaxies is unlikely.

3. The distribution of the parameter w shows that only in the k30 model there is a significant increase in density inside the halo, meaning they are more compact in this model than in other models. This is due to the fact that the scale of the peak corresponds to the typical masses of these halos: from 2×10^8 to $2 \times 10^9 M_\odot/h$.
4. In the k80 model, the halo parameters from the considered sample do not differ from those in Λ CDM.

5. CONCLUSION

This work demonstrates the possibility of studying the small-scale power spectrum of initial density perturbations by measuring the internal structure and spatial distribution of galaxies at high redshifts. Deviations of the spectrum

from the standard one (from the Λ CDM model) were set in the form of a Gaussian with a variable position. Numerical calculations of the formation of large-scale structure and dark matter halos were performed for five models: Λ CDM and 4 models with peak positions in the power spectrum at $k_0 = 7, 15, 30, 80 h/\text{Mpc}$.

Samples of halos from these models demonstrate the dependence of large-scale object distribution on the peak position: for models with $k_0 = 7$ and $k_0 = 15 h/\text{Mpc}$, an increased number of filaments is detected using the minimal spanning tree method. Additionally, in the model with $k_0 = 30 h/\text{Mpc}$, the distribution of branch lengths in the tree differs noticeably from the Λ CDM model, with a significantly lower number of filaments in the distribution of massive halos.

Models with $k_0 = 7, 15, 30 h/\text{Mpc}$ demonstrate increased values of the maximum circular velocity of halos (v_{max}) compared to Λ CDM, as well as somewhat more compact halos (with larger values of the parameter w) in the model with $k_0 = 30 h/\text{Mpc}$. The model with $k_0 = 80 h/\text{Mpc}$, based on the parameters we analyzed, does not differ from the Λ CDM model.

In the future, it is necessary to move from the analysis of dark halos to models of galaxies, for which one can use both simple semi-analytical models and hydrodynamic simulations with star formation. Having catalogs of model galaxies, it will become possible to build cones of model surveys for JWST, Millimetron, SKA, ALMA observatories, taking into account the peculiarities of galaxy selection by a particular observatory. As a result, it will be possible to provide predictions for observations on the expected parameters of the large-scale structure and galaxy parameters for models with the Λ CDM perturbation spectrum and models with a modified spectrum.

Also, although we set deviations from the Λ CDM model in the form of distortions of the power spectrum in the range $7 < k < 80 \text{ h/Mpc}$, which corresponds to scales $\lambda = 2\pi/k = 0.08 - 0.9 \text{ Mpc}/h$, this is not the only possible way to set additional small-scale perturbations in the same range of scales. If we abandon the requirement of Gaussianity of initial perturbations at small scales, they can be set in the form of separate density peaks (perturbations in r -space, not in k -space). It can be expected that with peak sizes in the range $0.1 - 1 \text{ Mpc}/h$, they will be able to form galaxies and supermassive black holes earlier than in the Λ CDM model (depending on the amplitude of the peaks). Similar models can also be investigated for their testability by observations using simulations.

6. ACKNOWLEDGMENTS

The authors are grateful to T.I. Larchenkova for moral support and D.I. Novikov for valuable discussions.

FUNDING

The work was supported by the LPI project NNG 41-2020.

CONFLICT OF INTEREST

The authors declare no conflict of interest.

REFERENCES

- R. Barkana and A. Loeb, *Physics Reports* **349** (2), 125 (2001).
- J. D. Barrow, S. P. Bhavsar, and D. H. Sonoda, *Monthly Notices Royal Astron. Soc.* **216**, 17 (1985).
- P. Behroozi and J. Silk, *Monthly Notices Royal Astron. Soc.* **477** (4), 5382 (2018).
- M. Boylan-Kolchin, *Nature Astronomy* **7**, 731 (2023).
- L. D. Bradley, D. Coe, G. Brammer, et al., *Astrophys. J.* **955** (1), 13 (2023).
- A. M. Brooks, M. Kuhlen, A. Zolotov, and D. Hooper, *Astrophys. J.* **765** (1), 22 (2013).
- G. L. Bryan and M. L. Norman, *Astrophys. J.* **495** (1), 80 (1998).
- M. Castellano, A. Fontana, T. Treu, et al., *Astrophys. J.* **938** (2), L15 (2022).
- S. Chabanier, M. Millea, and N. Palanque-Delabrouille, *Monthly Notices Royal Astron. Soc.* **489** (2), 2247 (2019).
- Y. Chen, H. J. Mo, and K. Wang, *arXiv e-prints arXiv:2304.13890* (2023).
- M. Demiański, A. Doroshkevich, T. Larchenkova, and S. Pilipenko, *Monthly Notices Royal Astron. Soc.* **525** (2), 1922 (2023).
- M. Demiański and A. G. Doroshkevich, *Astron. and Astrophys.* **422**, 423 (2004).
- M. I. Demiański, A. G. Doroshkevich, and T. I. Larchenkova, *Astronomy Letters* **48** (7), 361 (2022).
- G. Despali, C. Giocoli, R. E. Angulo, et al., *Monthly Notices Royal Astron. Soc.* **456** (3), 2486 (2016).
- C. T. Donnan, D. J. McLeod, J. S. Dunlop, et al., *Monthly Notices Royal Astron. Soc.* **518** (4), 6011 (2023).
- A. Doroshkevich, D. L. Tucker, S. Allam, and M. J. Way, *Astron. and Astrophys.* **418**, 7 (2004).
- A. G. Doroshkevich, D. L. Tucker, R. Fong, et al., *Monthly Notices Royal Astron. Soc.* **322** (2), 369 (2001).
- S. L. Finkelstein, M. B. Bagley, P. A. Haro, et al., *Astrophys. J.* **940** (2), L55 (2022).
- S. Giodini, D. Pierini, A. Finoguenov, et al., *The Astrophysical Journal* **703** (1), 982 (2009).
- Z. Haiman, T. Abel, and M. J. Rees, *Astrophys. J.* **534** (1), 11 (2000).
- E. R. Harrison, *Phys. Rev. D* **1** (10), 2726 (1970).
- K. Inomata, M. Braglia, and X. Chen, *Journal of Cosmology and Astroparticle Physics* **2023** (4), 011 (2023).
- P. Ivanov, P. Naselsky, and I. Novikov, *Phys. Rev. D* **50** (12), 7173 (1994).
- A. Klypin, A. V. Kravtsov, O. Valenzuela, and F. Prada, *Astrophys. J.* **522** (1), 82 (1999).

- A. A. Klypin, S. Trujillo-Gomez, and J. Primack, *The Astrophysical Journal* **740** (2), 102 (2011).
- A. Knebe, R. R. Islam, and J. Silk, *Monthly Notices Royal Astron. Soc.* **326** (1), 109 (2001).
- S. R. Knollmann and A. Knebe, *Astrophys. J. Suppl.* **182** (2), 608 (2009).
- I. Labbé, P. van Dokkum, E. Nelson, et al., *Nature* **616** (7956), 266 (2023).
- C. C. Lovell, I. Harrison, Y. Harikane, et al., *Monthly Notices of the Royal Astronomical Society* **518** (2), 2511 (2022).
- R. P. Naidu, P. A. Oesch, P. van Dokkum, et al., *Astrophys. J.* **940** (1), L14 (2022).
- H. Padmanabhan and A. Loeb, *The Astrophysical Journal Letters* **953** (1), L4 (2023).
- Planck Collaboration, N. Aghanim, Y. Akrami, et al., *Astron. and Astrophys.* **641**, A6 (2020).
- F. Prada, P. Behroozi, T. Ishiyama, et al., *arXiv e-prints arXiv:2304.11911* (2023).
- W. H. Press and P. Schechter, *Astrophys. J.* **187**, 425 (1974).
- P. Ralegankar, M. Pavičević, and M. Viel, *arXiv e-prints arXiv:2402.14079* (2024).
- T. Sawala, C. S. Frenk, A. Fattahi, et al., *Monthly Notices Royal Astron. Soc.* **456** (1), 85 (2016).
- X. Shen, M. Vogelsberger, M. Boylan-Kolchin, et al., *arXiv e-prints arXiv:2305.05679* (2023).
- R. K. Sheth and G. Tormen, *Monthly Notices Royal Astron. Soc.* **308** (1), 119 (1999).
- H. Sletmoen and H. A. Winther, *arXiv e-prints arXiv:2403.03786* (2024).
- V. Springel, *Monthly Notices Royal Astron. Soc.* **364**, 1105 (2005).
- M. V. Tkachev, S. V. Pilipenko, E. V. Mikheeva, and V. N. Lukash, *Monthly Notices Royal Astron. Soc.* **527** (1), 1381 (2024).
- F. Wang, J. Yang, J. F. Hennawi, et al., *Astrophys. J.* **951** (1), L4 (2023).
- M. Xiao, P. Oesch, D. Elbaz, et al., *arXiv e-prints arXiv:2309.02492* (2023).
- Y. B. Zel'dovich, *Astron. and Astrophys.* **5**, 84 (1970).
- Y. B. Zeldovich, *Monthly Notices Royal Astron. Soc.* **160**, 1P (1972).